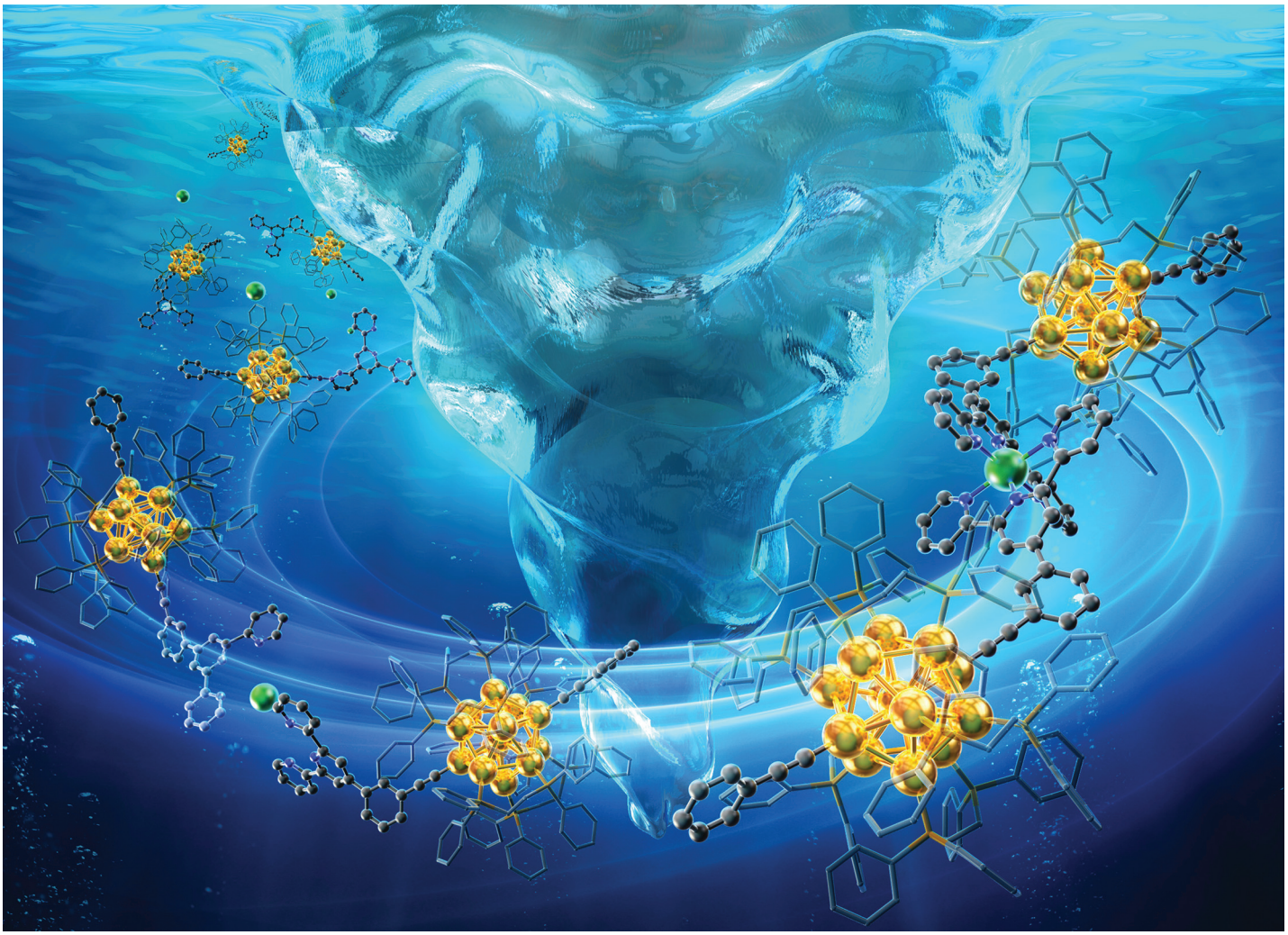

**Showcasing research from Prof. Yuichi Negishi's laboratory, Tohoku University, Japan.**

Synthesis of $Au_{13}$-based building block clusters for programmed dimer formation and $Au_{13}$ cluster dimer photoexcitation properties

This study demonstrates that the introduction of two types of ligands—chelating ligands that coordinate to the $Au_{13}$ cluster surface and end-capping ligands that suppress polymerization—enable the synthesis of building block molecules which are programmed to selectively and spontaneously form $Au_{13}$-based dimers upon the addition of metal ions. In the $Au_{13}$-based dimer, the rapid intramolecular photoinduced charge transfer occurred even with only a small driving force.

Image reproduced by permission of Yuichi Negishi from *Nanoscale*, 2025, **17**, 12695.

## As featured in:

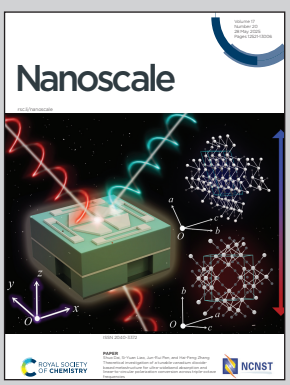


See Yoshiki Niihori, Yuichi Negishi *et al.*, *Nanoscale*, 2025, **17**, 12695.

ROYAL SOCIETY OF CHEMISTRY

rsc.li/nanoscale

Registered charity number: 207890

Nanoscale

PAPER

View Article Online
View Journal | View Issue



Cite this: *Nanoscale*, 2025, **17**, 12695

# Synthesis of $Au_{13}$-based building block clusters for programmed dimer formation and $Au_{13}$ cluster dimer photoexcitation properties†

Taiga Kosaka,[a] Yoshiki Niihori, *[b] Tokuhisa Kawawaki [c] and Yuichi Negishi *[c]

Recently, there has been increasing attention on the fabrication of ligand-protected metal clusters composed of a finite number of noble metal atoms and on their precise assembly to elicit novel properties that are not observed in individual metal clusters. In the present study, we investigated (1) the behavior of ligand exchange reactions and (2) the selective and efficient formation of dimers composed of $Au_{13}$ clusters. Specifically, we focused on a gold cluster consisting of 13 atoms coordinated to diphosphine ligands (dppe) and either chloride (Cl) or acetylide, *i.e.*, $[Au_{13}(dppe)_5X_2]^{3+}$ (X = Cl or acetylide). The findings showed that $Au_{13}$ clusters containing the counter anion $Cl^-$ undergo a transformation under specific conditions, where $Cl^-$ acts as a ligand (rather than an anion) directly coordinated to the $Au_{13}$ surface. The introduction of two types of ligands—chelating ligands that coordinate to the $Au_{13}$ cluster surface and end-capping ligands that suppress polymerization—enabled the synthesis of building block molecules that are programmed to selectively and spontaneously form $Au_{13}$-based dimers upon the addition of metal ions. The designed building block clusters indeed selectively and efficiently formed stable dimers composed of two $Au_{13}$ clusters in the presence of iron ions. Furthermore, in the $Au_{13}$-based dimer, the phosphorescent $Au_{13}$ moiety is directly connected to a coordination site that exhibits quenching effects, enabling rapid intramolecular photoinduced charge transfer even with a small driving force.

Received 18th February 2025,
Accepted 17th April 2025

DOI: 10.1039/d5nr00724k

rsc.li/nanoscale



## Introduction

Ligand-protected metal clusters, which consist of a finite number of noble metal atoms (such as gold and silver), exhibit size- or composition-dependent luminescence properties, magnetic behavior, and catalytic activity. Owing to these characteristics, they are expected to be applied in luminescent materials, magnetic memory devices, and oxidation catalysts.[1–6] The shape of the electronic orbitals in metal clusters resembles that of atomic orbitals (s, p, d, *etc.*). Therefore, metal clusters can be regarded as "superatoms".[7–17]

In recent years, three main approaches (Scheme S1†) have been explored for developing materials using superatoms as fundamental building units, *i.e.*: (1) fusing superatomic cores to form superatomic molecules;[18–35] (2) arranging and crystallizing metal clusters into superlattice structures, driven by interactions between surface ligands of adjacent clusters;[36–42] and (3) linking metal clusters through ligand exchange reactions with bridging ligands to form covalently bonded assemblies.[43–50] The materials obtained through these approaches exhibit absorption and emission properties,[19] as well as catalytic activity,[51] that differ from those of individual metal clusters. Consequently, the fabrication of materials using metal clusters as building units has garnered attention as an effective strategy for unlocking novel properties based on metal clusters. However, core fusion between metal clusters in approach (1) is complex, thereby hindering its universal application to different systems. In approach (2), where crystal growth is driven by isotropic interactions between metal cluster surfaces, only a limited range of packing structures can be achieved.[52,53] In approach (3), where metal clusters are linked *via* ligand exchange reactions, reaction control is challenging, often leading to the formation of randomly connected assemblies or amorphous polymers with multiple linkages.[54] Therefore, designing and precisely synthesizing metal cluster assemblies with the desired structures using approaches (1)–(3) is a significant challenge.

In this context, to explore alternative methods of linking, research has recently focused on introducing acetylide ligands

[a]*Department of Chemistry, Graduate School of Science, Tokyo University of Science, 1-3 Kagurazaka, Shinjuku-ku, Tokyo 162-8601, Japan*
[b]*Research Institute for Science & Technology, Tokyo University of Science, 1-3 Kagurazaka, Shinjuku-ku, Tokyo 162-8601, Japan. E-mail: niihori@rs.tus.ac.jp*
[c]*Institute of Multidisciplinary Research for Advanced Materials, Tohoku University, 2-1-1 Katahira, Aoba-ku, Sendai 980-8577, Japan. E-mail: yuichi.negishi.a8@tohoku.ac.jp*

†Electronic supplementary information (ESI) available. See DOI: https://doi.org/10.1039/d5nr00724k

and their analogs into gold (Au) clusters. The Au clusters are coordinated by diverse types of ligands, such as phosphines and halogens, through ligand exchange reactions.[55–67] For example, Tsukuda *et al.* synthesized a building block superatom by exchanging the two terminal chlorine ligands of $[Au_{13}(dppe)_5Cl_2]^{3+}$ (hereafter referred to as **1**; dppe = 1,2-bis(diphenylphosphino)ethane) (Table 1 and Fig. S1A†) with terpyridine derivative acetylide ligands (chelating ligands), thereby introducing terpyridine (EPTpy = 4′-(4-ethynylphenyl)-2,2′:6′,2″-terpyridine) at both ends of the $Au_{13}$ cluster. This exchange subsequently enabled the formation of a one-dimensional polymer upon the addition of transition metal ions into the solution containing the building block superatom, wherein the metal ions coordinated with terpyridine, which led to the formation of $Au_{13}$ cluster-linked polymer chains (Scheme 1A).[68] Additionally, $(IrAu_{12})_2L$ dimers and $(IrAu_{12})_3L_2$ trimers were synthesized using the analogous compound $[IrAu_{12}(dppe)_5(PA)_2]^+$ (PA = phenylacetylide; Fig. S2A†) to control the cleavage of the Au–C bond (dissociation of PA) within the cluster and by introducing the diisocyanide linker L, which has isocyano groups at both ends (Scheme 1B).[56] The approach shown in Scheme 1A affords the facile synthesis of one-dimensional assemblies by simply introducing transition metal ions. However, controlling the number of linkages is difficult. In contrast, the approach in Scheme 1B allows for control of the number of linkages in the product by combining clusters where PA is dissociated from the clusters, with one PA remaining as an end cap to suppress polymerization. However, the number of strong acid reagents suitable for PA dissociation is limited, which restricts the types of clusters that can be used for linking.

In the present study, we developed an alternative approach that focuses on driving the formation of oligomers through simple coordination between chelating ligands and transition metal ions. By introducing chelating ligands to the Au cluster surface and end-capping ligands to suppress polymerization, we developed building block molecules programmed to self-assemble into dimers upon the addition of metal ions (Scheme 1C). Indeed, the designed building block clusters efficiently formed stable dimers consisting of two Au clusters in the presence of iron ions. Furthermore, the dimers have been shown to exhibit a photo-induced charge transfer property.

**Table 1** Chemical formulae and identification numbers of **1–3**

| Number | Chemical formula |
|---|---|
| **1** | $[Au_{13}(dppe)_5Cl_2]^{3+}$ |
| $\mathbf{2_0}$ | $[Au_{13}(dppe)_5(PA)_2]^{3+}$ |
| $\mathbf{2_1}$ | $[Au_{13}(dppe)_5(PA)(C_2PhTpy)]^{3+}$ |
| $\mathbf{2_2}$ | $[Au_{13}(dppe)_5(C_2PhTpy)_2]^{3+}$ |
| **3** | $[Fe(TpyPhC_2H)_2]^{2+}$ |

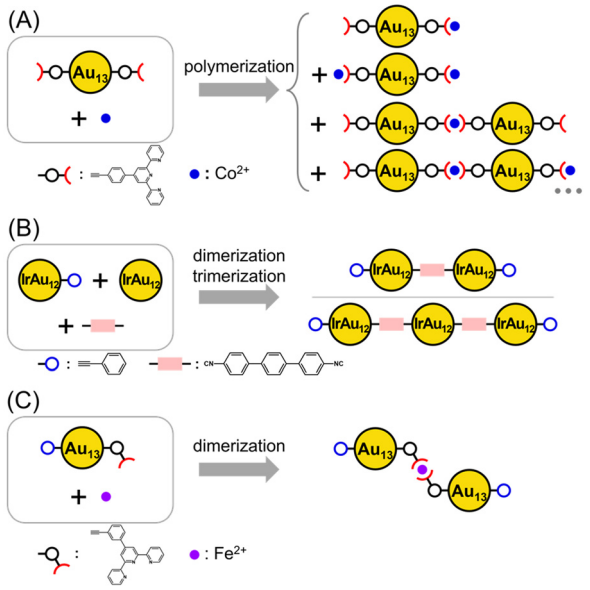


**Scheme 1** Synthesis strategies of the $Au_{13}$-based cluster linkage. (A) Polymer formation through coordination bonds between transition metal ions and chelating ligands.[68] (B) Au atom exposure by selective desorption of halogen and dimer and trimer formation by reaction with an isocyanide linker.[56] (C) Selective dimer formation by complexation with building block molecules containing end-cap ligands and chelating ligands programmed to form dimers (this work).

## Experimental

### Synthesis of $\mathbf{1}\cdot(BF_4^-)_3$

First, the precursor complex $Au_2Cl_2(dppe)$ was synthesized using a method reported by Corma *et al.*[69] Specifically, 350 μmol of tetrachloroauric acid was dissolved in 2.5 mL of methanol. To this solution, 109 μL (1.05 mmol) of thiodiglycol, dissolved in 500 μL of methanol, was added, and the reaction mixture was stirred at room temperature for 1 h. After the solution changed from yellow to colorless and transparent, 69.7 mg (175 μmol) of dppe, dissolved in 4 mL of a chloroform : toluene (1 : 1 v/v) mixed solvent, was added, and the mixture was stirred at room temperature for 2 h. The resulting white precipitate was washed with methanol to yield $Au_2Cl_2(dppe)$.

Next, $\mathbf{1}\cdot(Cl^-)_3$ (Fig. S1A†) was synthesized using a method from the literature[13] but without the addition of sodium sulfide. Specifically, 126 mg (100 μmol) of $Au_2Cl_2(dppe)$ was added to 20 mL of dichloromethane. To this solution, a sodium borohydride aqueous solution (3.8 mg (100 μmol) per 1 mL) at 0 °C was added. The solution was then stirred at room temperature for 24 h. After evaporating the solvent, the resulting solid was washed with water, a hexane/dichloromethane mixture, and acetone to yield $\mathbf{1}\cdot(Cl^-)_3$ (Fig. S3 (curve a)†). The obtained $\mathbf{1}\cdot(Cl^-)_3$ was dissolved in ethanol, and an excess of sodium tetrafluoroborate was added to exchange the counter anion from $Cl^-$ to $BF_4^-$, yielding $\mathbf{1}\cdot(BF_4^-)_3$ as a powder (Fig. S3 (curve b)†).[12,13]

### Formation of dimers *via* complex formation

The acetylene derivative 4′-(3-ethynylphenyl)-2,2′:6′,2″-terpyridine (H-$C_2$PhTpy) (Fig. S2B†), which contains a terpyridine unit that can coordinate with transition metal ions, was synthesized in the following three steps.[70–72] The details of the organic synthesis are provided in the ESI.† First, the terpyridine framework (–PhTpy) was formed *via* Kröhnke pyridine synthesis using 3-bromobenzaldehyde, 2-acetylpyridine, and ammonia (Fig. S4A†). Next, the Sonogashira coupling reaction was used to introduce a trimethylsilylethynyl group at the 3-position of the phenylene ring (Fig. S4B†). Finally, the trimethylsilyl protecting group was removed using fluoride ions, yielding the white target compound H-$C_2$PhTpy (Fig. S4C†) with a final yield of 13%.

To prevent the formation of polymers larger than dimers, owing to coordination, we synthesized a $Au_{13}$ cluster (building block cluster; BB cluster) containing H-$C_2$PhTpy and the end-cap ligand phenylacetylene (H-PA). Specifically, 6.8 mg (1.39 μmol) of **1**·$(BF_4^-)_3$ was dissolved in 33.4 mL of acetonitrile. To this solution, 19.4 μL (139 μmol) of triethylamine, 13.8 μL (126 μmol) of H-PA, and 4.6 mg (13.8 μmol) of H-$C_2$PhTpy were added, and the solution was stirred (concentration ratio **1** : H-PA : H-$C_2$PhTpy = 1 : 90 : 10 or 1 : 74 : 26). Using this method, the BB cluster $[Au_{13}(dppe)_5(PA)_{2-x}(C_2PhTpy)_x]^{3+}$ (where $x$ = 0–2; hereafter referred to as $\mathbf{2_0}$ ($x$ = 0; Fig. S1B†), $\mathbf{2_1}$ ($x$ = 1; Fig. S1C†), and $\mathbf{2_2}$ ($x$ = 2); Table 1) was obtained, in which two types of acetylide ligands were introduced to the surface of the $Au_{13}$ cluster.

The obtained BB cluster was dissolved in acetonitrile, and a solution of iron(II) tetrafluoroborate ($Fe(BF_4^-)_2$) in acetonitrile (12.3 μM) was added. Complex formation was monitored using ultraviolet–visible (UV–vis) absorption spectroscopy. The chemical composition of the products after complexation was evaluated by mass spectrometry. For products obtained by adding $Fe(BF_4^-)_2$ in excess of the equivalence point, mass spectrometry was conducted after removing excess $Fe^{2+}$.

### Evaluation of luminescence lifetime and quenching experiments

The luminescence decay curves of the dimers obtained from complexation were obtained using a pico-TAS system from UNISOKU (Hirakata City, Osaka, Japan). Excitation light with a wavelength of 520 nm was used. Prior to the measurements, the solutions were deoxygenated by argon bubbling. The primary objective of the measurement was to observe the photoinduced charge transfer behavior of the BB cluster. The $Fe^{2+}$ terpyridine complex $[Fe(TpyPhC_2H)_2](BF_4^-)_2$, hereafter referred to as **3**·$(BF_4^-)_2$ (Table 1 and Fig. S5†), was used as the quenching agent to quench the luminescence of the $Au_{13}$ component.

### Formation of dimers *via* the introduction of a diyne

An attempt was also made to synthesize a linkage of $Au_{13}$ clusters by reacting compound **1** with a diyne having ethynyl groups at both ends (Scheme S2B†). Specifically, 49 mg (10 μmol) of **1**·$(Cl^-)_3$ was dissolved in 33 mL of acetonitrile. To this solution, 1.3 mg (10 μmol) of 1,4-diethynylbenzene (deb-$H_2$; Fig. S2C†) and 14 μL (100 μmol) of triethylamine were added, followed by stirring the solution ([**1**] : [deb-$H_2$] = 1 : 1). The solution was then dried, and excess ligands, bases, and impurities were washed with water, hexane, and toluene. The chemical composition of the obtained product was evaluated by mass spectrometry.

## Results and discussion

### Influence of counter ions on ligand exchange reactions

We first discuss the effect of the counteranion type on the ligand exchange reaction.

Fig. 1 shows the electrospray ionization (ESI) mass spectra of $\mathbf{2_0}$·$(Cl^-)_3$ (Fig. S1B and S3 (curve c)†) and the product obtained by mixing $\mathbf{2_0}$·$(Cl^-)_3$ with $Fe(BF_4^-)_2$. The mass spectrum of the product featured peaks corresponding to $[Au_{13}(dppe)_5(PA)_{2-x}Cl_x](BF_4^-)_3$ ($x$ = 0–2). This finding indicates that during the reaction, ligand exchange occurred between the counteranion $Cl^-$ of the $Au_{13}$ cluster and PA (eqn (1)).

$$[Au_{13}(dppe)_5(PA)_2](Cl^-)_3 \xrightarrow{[BF_4]^-} [Au_{13}(dppe)_5(PA)_{2-x}Cl_x](BF_4^-)_3 \quad (1)$$

Thus, (1) the $Cl^-$ changes its role from a counteranion to a ligand depending on the reaction conditions and (2) under conditions where $Cl^-$ ions are present, ligand exchange occurs from the acetylide ligand to $Cl^-$.

To achieve dimerization *via* complexation, it is essential to introduce only $Fe(BF_4^-)_2$ into the system, while maintaining the structure of the BB cluster. To suppress the occurrence of the aforementioned ligand exchange during mixing, $[BF_4]^-$ was consistently used as a counteranion of the precursor $Au_{13}$ cluster (*e.g.*, **1**·$(BF_4^-)_3$ and $\mathbf{2_{0-1}}$·$(BF_4^-)_3$). In the experiment, the addition of $NaBF_4$ to an ethanol solution of **1**·$(Cl^-)_3$ induced counteranion exchange and changes in the solubility of the cluster, resulting in the precipitation of **1**·$(BF_4^-)_3$ (Fig. S3 (curve b)†).

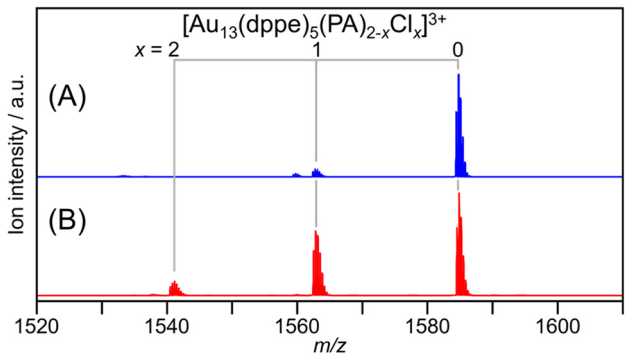


**Fig. 1** Positive-ion ESI mass spectra of (A) $\mathbf{2_0}$·$(Cl^-)_3$ and (B) the product obtained by mixing $\mathbf{2_0}$·$(Cl^-)_3$ and $[BF_4]^-$ in acetonitrile solution.

### Formation of dimers *via* complex formation

Fig. 2A (curve a) shows the ESI mass spectrum of the product obtained by adding H-PA and H-$C_2$PhTpy to an acetonitrile solution of $\mathbf{1}\cdot(BF_4^-)_3$ in the presence of a base (triethylamine). The mass spectrum mainly exhibited peaks attributed to $\mathbf{2_0}$ and $\mathbf{2_1}$. This result confirms that two $Cl^-$ ligands on the $Au_{13}$ cluster surface were substituted by PA or $C_2$PhTpy. When $C_2$PhTpy was introduced more excessively, $\mathbf{2_2}$ formed and the subsequent addition of $Fe^{2+}$ could result in the formation of dimers or larger assemblies (Scheme S2A†). Therefore, during the synthesis of the BB cluster, the molar ratio of acetylide ligands to H-PA : H-$C_2$PhTpy was set to 0.9 : 0.1 to minimize the formation of $\mathbf{2_2}$, while achieving the desired formation of $\mathbf{2_1}$ (Fig. S6 and Table S1†).

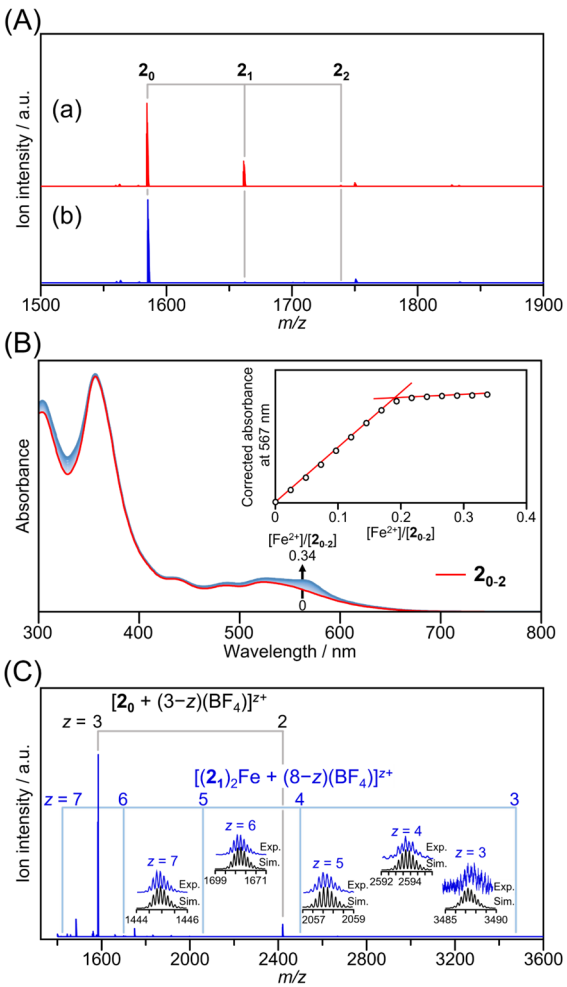


**Fig. 2** (A) ESI mass spectra of the BB cluster containing $\mathbf{2_{0-2}}$ prepared at a H-PA : H-$C_2$PhTpy molar ratio of 0.9 : 0.1 (a) and the product obtained from the reaction between the BB cluster containing $\mathbf{2_{0-2}}$ and $Fe(BF_4^-)_2$ (b). (B) UV–vis absorption spectra of the BB cluster containing $\mathbf{2_{0-2}}$ as a function of concentration of $Fe(BF_4^-)_2$. The inset shows the titration curve monitored at the characteristic absorption peak of 567 nm, which can be attributed to the MLCT transition of the $[Fe(Tpy)_2]^{2+}$ moiety. (C) Wide-range ESI mass spectrum of the product obtained from the reaction between the BB cluster containing $\mathbf{2_{0-2}}$ and $Fe(BF_4^-)_2$.

The composition distribution of the ligands in the obtained products differed from the binomial distribution predicted from the molar ratio of ligands added during synthesis (Fig. S6 and Table S2†). This result indicates that there is a difference in the ligand exchange ability between the two types of acetylide ligands used in this study. The observed deviation suggests that $C_2$PhTpy is more likely to replace the $Cl^-$ ligand of the $Au_{13}$ cluster than PA. $C_2$PhTpy has a bulkier geometric structure than PA (Fig. S2A and B†). Nevertheless, $C_2$PhTpy is more easily introduced into the $Au_{13}$ cluster than PA, which is attributed to the difference in the ease of proton dissociation of the acetylene groups ($pK_a$) of both ligands. The $^1$H NMR measurements revealed that the NMR shifts of the acetylene (H–C≡C) protons in H-$C_2$PhTpy and H-PA were 3.15 ppm (Fig. S4C†) and 3.07 ppm (TCI Product Number: 3RJHI), respectively, indicating that the electron density of the hydrogen in H-$C_2$PhTpy is lower than in H-PA. This suggests that H-$C_2$PhTpy more readily deprotonates than H-PA. This difference makes H-$C_2$PhTpy more nucleophilic than H-PA and more likely to attack the $Au_{13}$ core; therefore, H-$C_2$PhTpy is more readily incorporated into the $Au_{13}$ cluster than H-PA.

Fig. 2B shows the optical absorption spectrum of the BB cluster (red line). The absorption profile is comparable to those previously reported for $\mathbf{2_0}\cdot(PF_6^-)_3$ and $[Au_{13}(dppe)_5(EPTpy)_2]\cdot(PF_6)_3$.[55,68] This similarity indicates that the structure of the terminal functional groups of the acetylide ligands has little effect on the optical absorption properties of the cluster.

The addition of an $Fe(BF_4^-)_2$ acetonitrile solution to the BB cluster containing $\mathbf{2_{0-2}}$ resulted in an increase in absorbance at ~567 nm (Fig. 2B). The peak displayed a comparable shape and absorption wavelength to the metal-to-ligand charge transfer (MLCT) absorption peak of $[Fe(Tpy)_2]^{2+}$, which is formed by $Fe^{2+}$ and two Tpy molecules. This result suggests that the addition of $Fe^{2+}$ led to the formation of a complex between $Fe^{2+}$ and the Tpy sites of $\mathbf{2_1}$.

The inset in Fig. 2B illustrates the correlation between the concentration ratio $[Fe^{2+}]/[\mathbf{2_{0-2}}]$ and the absorbance at ~567 nm. As the $[Fe^{2+}]/[\mathbf{2_{0-2}}]$ ratio increased, the absorbance increased linearly up to $[Fe^{2+}]/[\mathbf{2_{0-2}}] = 0.18$, after which there was no increase or decrease in absorbance. This result suggests that $[Fe^{2+}]/[\mathbf{2_{0-2}}] = 0.18$ represents the equivalence point of complex formation ($[Fe^{2+}]/[\mathbf{2_{0-2}}]_{eq.}$). Typically, for the formation of $[Fe(Tpy)_2]$ from $Fe^{2+}$ and two Tpy molecules, the equivalence point is at $[Fe^{2+}]/[Tpy]_{eq.} = 0.5$.[73] However, because the products obtained in this study mainly consist of $\mathbf{2_0}$ and $\mathbf{2_1}$, the equivalence point is lower. By introducing the composition distribution obtained from the ESI mass spectrometry data into the stoichiometric equation (eqn (S10)†), a value of $[Fe^{2+}]/[\mathbf{2_{0-2}}]_{eq.} = 0.13$ is obtained. This value is in relatively good agreement with the value of $[Fe^{2+}]/[\mathbf{2_{0-2}}]_{eq.} = 0.18$ determined from the absorbance measurements, suggesting that $\mathbf{2_1}$, formed through ligand exchange, efficiently complexes with $Fe^{2+}$.

Fig. 2A (curve b) shows the mass spectrum of the product obtained after adding an excess amount of $Fe(BF_4^-)_2$ beyond the equivalence point and removing excess $Fe^{2+}$. The peak corresponding to $\mathbf{2_1}$ was absent and only the peak corresponding to unreacted $\mathbf{2_0}$ remained. When examining the mass spectrum over a broader range, peaks attributed to $[(\mathbf{2_1})_2Fe + (8 - z)(BF_4)]^{z+}$ ($z$ = 3–7) were observed in the high mass-to-charge ($m/z$) ratio region (Fig. 2C). These peaks correspond to $Au_{13}$ dimers formed by the complexation of $Fe^{2+}$ with two $\mathbf{2_1}$ units. For example, the charge state of +7 of the dimer molecule can be explained by a combination of two $Au_{13}$ units with a charge of +3, one Fe ion with a charge of +2, and one counteranion $[BF_4]^-$. Since the product used in this study (Fig. 2A, curve a) contains little of compound $\mathbf{2_2}$, which is capable of forming higher-order assemblies, oligomers such as trimers ($n$ = 3) or tetramers ($n$ = 4), represented as $(\mathbf{2_1})_2(\mathbf{2_2})_{n-2}Fe_{n-1}$ ($n \geq 3$), were scarcely observed in the mass spectrum. These results indicate that BB clusters were successfully designed to selectively form dimers as the connected structure by simply adding $Fe^{2+}$ (Fig. S7†).

The $Au_{13}$ cluster carries a charge of +3, and during dimer formation, there should be electrostatic repulsion between the $Au_{13}$ units as well as between the $Fe^{2+}$ ions. However, the stability constant ($\beta$) for the complexation between $Fe^{2+}$ and Tpy, $Fe^{2+} + 2Tpy \rightleftarrows [Fe(Tpy)_2]$, is large ($\beta = 10^{20.9}$ $M^{-2}$),[74] indicating that complex formation is thermodynamically favorable. This large stability constant likely contributes to the efficient formation of dimers through complexation despite electrostatic repulsion. This thermodynamic driving force enables the successful formation of dimers despite competing repulsive interactions.

The formation of dimers *via* complexation was achieved but the ion intensity of the dimer in the mass spectrum was weak. These dimers have a significantly larger mass than the monomer, which reduces their detection efficiency in mass spectrometry. Additionally, because $[BF_4]^-$ attached to the dimer with various combinations, the peaks originating from the dimer were observed across a range of $m/z$ ratios. Furthermore, the addition of $[BF_4]^-$ causes a widening of the isotope distribution, further decreasing the apparent intensity of the peaks. For example, in Fig. 2C, peaks corresponding to the addition of 1–5 $[BF_4]^-$ ions to the dimer were observed, resulting in charge states ranging from +3 to +7. These factors contribute to the apparent low yield of the dimer in the mass spectrum. However, from the data in Fig. 2A (curve b) and Fig. 2B, we estimate that all $\mathbf{2_1}$ units included in the mixture with a 24.4% molar ratio were likely forming dimers at the equivalence point of $[Fe^{2+}]/[\mathbf{2_{0-2}}] = 0.18$.

### Photoexcitation characteristics of dimers

To investigate the photophysical properties of the synthesized $(\mathbf{2_1})_2Fe$ dimer, its luminescence decay curve was evaluated. Fig. 3A shows the emission decay curve of the sample containing $\mathbf{2_0}$ and $(\mathbf{2_1})_2Fe$. The experimentally obtained decay curve could be fitted to a biexponential decay model with short and long lifetime components of 7.8 ns and 3.5 μs, respectively. To identify these two emission species, the luminescence lifetime of the BB cluster was evaluated. The emission decay of the BB cluster could be fitted to a nearly single exponential decay, with a lifetime of 3.5 μs (Fig. 3B). This value is consistent with the long-lived component observed in the sample containing $\mathbf{2_0}$ and $(\mathbf{2_1})_2Fe$. Therefore, the luminescence lifetime of $(\mathbf{2_1})_2Fe$ can be assigned as 7.8 ns. This value is comparable to that reported by Tsukuda *et al.* for a one-dimensional polymer composed of $Au_{13}$ and $Co^{2+}$, which supports the validity of this assignment.[68] From these results, the following conclusions can be drawn: (1) the luminescence lifetime of the BB cluster remains roughly constant and is independent of the type of acetylide ligand;[55] (2) quenching of the $Au_{13}$-derived luminescence occurs upon complex formation between $\mathbf{2_1}$ and $Fe^{2+}$; and (3) in the presence of $(\mathbf{2_1})_2Fe$ containing $Fe(Tpy)_2$ moieties, the $\mathbf{2_0}$ luminescence is not quenched.

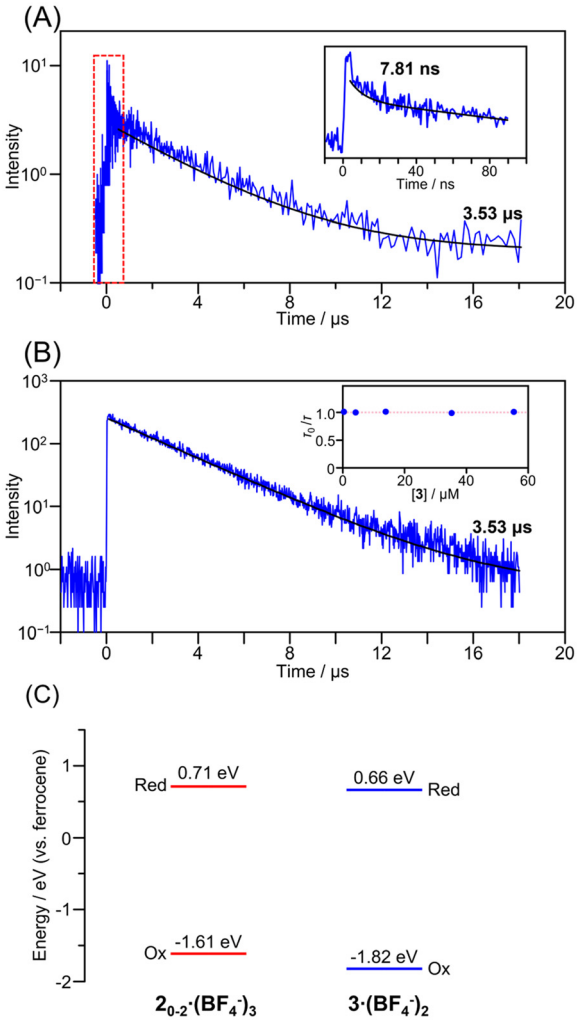


**Fig. 3** (A) Photoluminescence decay curve of the sample containing the $\mathbf{2_0}$ monomer and the $(\mathbf{2_1})_2Fe$ dimer. The inset shows an enlarged decay curve around 0–80 ns. (B) Photoluminescence decay curve of the building block cluster $\mathbf{2_{0-2}}$. The inset shows the Stern–Volmer plot based on the luminescence lifetimes of $\mathbf{2_{0-2}}$ in the presence of **3** as a quencher. (C) Redox potentials of $\mathbf{2_{0-2}}\cdot(BF_4^-)_3$ and $\mathbf{3}\cdot(BF_4^-)_2$.

Previous reports on $Au_{13}$ clusters, such as $Au_{13}(dppe)_5(EPTPy)_2$ and transition metal ions ($Ni^{2+}$, $Co^{2+}$, $Cu^{2+}$), have shown that the luminescence intensity and lifetime of $Au_{13}$ decrease upon complexation.[68] This phenomenon is believed to be due to the energy transfer from the excited state of $Au_{13}$ to the transition metal ion. In our study of the complexation between $\mathbf{2_1}$ and $Fe^{2+}$, the MLCT transition of $[Fe(Tpy)_2]^{2+}$ was observed in the long-wavelength region, but there was no significant overlap with the $Au_{13}$ emission spectrum in that absorption wavelength region (Fig. S8†). Therefore, the quenching observed upon $Fe^{2+}$ complexation of $\mathbf{2_1}$ is likely due to photoinduced charge transfer, rather than Förster-type resonance energy transfer.[75] Our present study reveals that $[Fe(Tpy)_2]^{2+}$ can act as a charge transfer quencher for $Au_{13}$ luminescence. However, as mentioned earlier, $\mathbf{2_0}$ is not quenched by the coexisting complex component $(\mathbf{2_1})_2Fe$ dimer.

To confirm this, a quenching experiment was conducted using $\mathbf{3}\cdot(BF_4^-)_2$, which has a similar structure to that of the constituent unit of the dimer, as the quencher against the $\mathbf{2_{0-2}}$-containing BB cluster (Fig. 3B inset and Fig. S9†). Although attempts were made to observe quenching using steady-state luminescence, the absorption band of **3** overlapped with the entire absorption spectrum of $\mathbf{2_{0-2}}$, resulting in a decrease in emission intensity owing to the excitation inner filter effect. Therefore, steady-state emission quenching experiments were deemed inappropriate. In contrast, time-correlated single-photon counting measurements of the emission decay confirmed that the emission lifetime of $\mathbf{2_{0-2}}$ remained constant regardless of the concentration of **3** (Fig. S10†). This finding indicates that **3** does not act as a quencher for $\mathbf{2_{0-2}}$, and considering the redox potentials of $\mathbf{2_{0-2}}\cdot(BF_4^-)_3$ and $\mathbf{3}\cdot(BF_4^-)_2$, it is evident that the driving force for photoinduced electron transfer from $\mathbf{2_{0-2}}$ to **3** is very small (Fig. 3C and Fig. S11†). Therefore, the drastic decrease in emission lifetime due to dimerization can be attributed to the shortening of the excited-state of $Au_{13}$, which results from the chemical direct binding of a metal complex to the emission site of $Au_{13}$. Although the driving force is small, the metal complex has the potential to act as a quenching site. This finding demonstrates that even combinations of clusters and transition metal ions that would not typically cause quenching can cause photoinduced charge transfer in molecules created by the linkage of these moieties, thereby enabling luminescence quenching.

### Formation of dimers *via* the introduction of a diyne

We also examined a different method to synthesize the linkage. An attempt was made to synthesize a linkage of $Au_{13}$ clusters by reacting compound **1** with a diyne having ethynyl groups at both ends (Scheme S2B†). Fig. 4 shows the ESI mass spectrum of the product obtained by adding deb-$H_2$ (Fig. S2C†) to an acetonitrile solution of $\mathbf{1}\cdot(BF_4^-)_3$ in the presence of a base (triethylamine). The peak with the strongest ion intensity was attributed to $[Au_{13}(dppe)_5(deb\text{-}H)_2]^{3+}$. This result indicates that the Cl ligands on the $Au_{13}$ surface were substituted by the $[deb\text{-}H]^-$ anion generated through deprotonation of one of the hydrogens of deb-$H_2$ by the base. In contrast, no

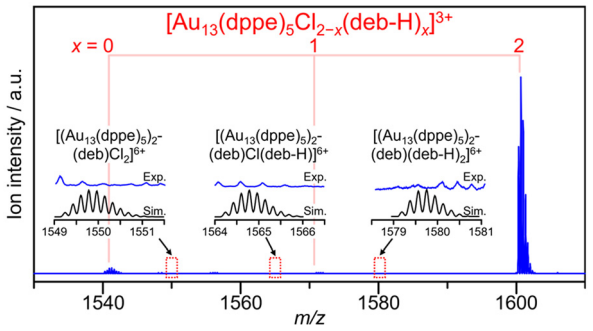


**Fig. 4** Positive-ion ESI mass spectrum of the product obtained by mixing **1** and deb-$H_2$ in acetonitrile solution in the presence of a base.

distinct peaks were observed in the expected *m*/*z* range (1550, 1565, 1580) associated with dimer formation. If both terminal hydrogens of [deb-$H_2$] are deprotonated by the base, $[deb]^{2-}$ is expected to replace one Cl on each $Au_{13}$ cluster, forming the desired dimer. However, if both Cl ligands on each $Au_{13}$ cluster are replaced by $[deb]^{2-}$, this would lead to the formation of a polymer connecting multiple $Au_{13}$ clusters (Scheme S2B†). As the reaction proceeded to form structures linking many $Au_{13}$ clusters, we conclude that selective formation of the desired dimer cannot be achieved using this method.

Accordingly, we speculated that selective dimer formation might be possible by replacing one of the Cl ligands of **1** with PA, forming $Au_{13}(dppe)_5Cl(PA)$. However, the findings revealed that ligand exchange occurred between the halogen and acetylide ligands, as well as between the different acetylides on the $Au_{13}$ cluster (Fig. S12†). To examine the ligand exchange ability of the acetylide ligands, a model experiment was conducted by adding deb-$H_2$ and triethylamine to $\mathbf{2_0}\cdot(Cl^-)_3$ (Fig. S1B and S3 (curve c)†). As observed in Fig. S12,† the mass spectrum of the product featured peaks corresponding to $[Au_{13}(dppe)_5(PA)_{2-x}(deb\text{-}H)_x]^{3+}$. This indicates that ligand exchange reactions occur even between acetylide ligands, and that ligand exchange reactions involving halogens or acetylides on the $Au_{13}$ cluster are reversible, similarly to thiol or thiolate exchange reactions in thiolate-protected Au clusters such as $Au_{25}(SR)_{18}$.[57,76–80] Therefore, control over the reaction and selective formation of the desired linkage structure is difficult using bridging ligands such as deb-$H_2$. In contrast, the approach using the aforementioned complexation and end-cap ligands is a more straightforward and precise synthetic approach.

## Conclusions

In this study, we focused on $Au_{13}$ clusters with phosphine ligands and chlorine or acetylide as the coordinating ligands, $[Au_{13}(dppe)_5X_2]^{3+}$ (X = Cl or acetylide), to investigate (1) the behavior of ligand exchange reactions and (2) the development of selective and efficient methods for the formation of dimers

using $Au_{13}$ clusters. The following key findings were obtained. (1) Under certain conditions, $Au_{13}$ clusters with $Cl^-$ as a counteranion can undergo a transformation where $Cl^-$ no longer acts as the counteranion but instead directly binds to the $Au_{13}$ surface as a coordinating ligand. (2) The introduction of two types of ligands—chelating ligands that can complex and end-cap ligands that can suppress polymerization—resulted in the development of building block clusters that were programmed to form dimers consisting of two $Au_{13}$ clusters. By applying $Fe^{2+}$ ions to these designed building block clusters, we succeeded in efficiently forming a dimer consisting of two $Au_{13}$ molecules. Furthermore, these dimers, having a charge donor and acceptor chemically bound together, displayed a higher rate constant for light-induced charge transfer than typical endothermic complexes. Future studies are expected to further investigate the new properties resulting from dimerization.

## Author contributions

Y. Niihori and Y. Negishi conceived the idea for this study and supervised the project. T. Kosaka and Y. Niihori conducted the synthesis and characterization. T. Kosaka, T. Kawawaki and Y. Niihori wrote the manuscript and Y. Negishi revised the manuscript. All authors discussed the results and approved the final version of the manuscript.

## Data availability

Relevant data are available from the corresponding authors (Y. Niihori and Y. Negishi) upon reasonable request.

## Conflicts of interest

The authors have no conflicts to declare.

## Acknowledgements

We gratefully acknowledge Mr Ryusei Kaneko and Prof. Shinichi Saito (Tokyo University of Science) for supporting the synthesis of terpyridine derivatives. We thank Dr Tatsuo Nakagawa and Toshiaki Suzuki in UNISOKU Co., Ltd, for conducting the measurement of the photoluminescence decay curves. Computation was performed at the Research Center for Computational Science, Okazaki, Japan (project no. 24-IMS-C282). This research was financially supported by the Japan Society for the Promotion of Science (JSPS) KAKENHI (grant no. 22K04858, 22K19012, 23KK0098, and 23H00289), the Yazaki Memorial Foundation for Science and Technology, and The Sumitomo Foundation.

## References

1 Y. Shichibu, Y. Negishi, H. Tsunoyama, M. Kanehara, T. Teranishi and T. Tsukuda, *Small*, 2007, **3**, 835–839.
2 R. Jin, H. Qian, Z. Wu, Y. Zhu, M. Zhu, A. Mohanty and N. Garg, *J. Phys. Chem. Lett.*, 2010, **1**, 2903–2910.
3 Y. Shichibu, Y. Negishi, T. Tsukuda and T. Teranishi, *J. Am. Chem. Soc.*, 2005, **127**, 13464–13465.
4 Y. Negishi, T. Nakazaki, S. Malola, S. Takano, Y. Niihori, W. Kurashige, S. Yamazoe, T. Tsukuda and H. Häkkinen, *J. Am. Chem. Soc.*, 2015, **137**, 1206–1212.
5 K. Kwak, Q. Tang, M. Kim, D.-E. Jiang and D. Lee, *J. Am. Chem. Soc.*, 2015, **137**, 10833–10840.
6 G. Li and R. Jin, *Acc. Chem. Res.*, 2013, **46**, 1749–1758.
7 J.-I. Nishigaki, K. Koyasu and T. Tsukuda, *Chem. Rec.*, 2014, **14**, 897–909.
8 D. M. P. Mingos, *Dalton Trans.*, 2015, **44**, 6680–6695.
9 L. Cheng and J. Yang, *J. Chem. Phys.*, 2013, **138**, 141101.
10 B. K. Teo and H. Zhang, *Coord. Chem. Rev.*, 1995, **143**, 611–636.
11 C. E. Briant, B. R. C. Theobald, J. W. White, L. K. Bell, D. M. P. Mingos and A. J. Welch, *J. Chem. Soc., Chem. Commun.*, 1981, 201–202.
12 Y. Shichibu and K. Konishi, *Small*, 2010, **6**, 1216–1220.
13 J. Zhang, Y. Zhou, K. Zheng, H. Abroshan, D. R. Kauffman, J. Sun and G. Li, *Nano Res.*, 2018, **11**, 5787–5798.
14 R. C. B. Copley and D. M. P. Mingos, *J. Chem. Soc., Dalton Trans.*, 1996, 491–500.
15 R. C. B. Copley and D. M. P. Mingos, *J. Chem. Soc., Dalton Trans.*, 1992, 1755–1756.
16 M. Laupp and J. Strähle, *Angew. Chem., Int. Ed. Engl.*, 1994, **33**, 207–209.
17 X. Kang, L. Xiong, S. Wang, Y. Pei and M. Zhu, *Chem. Commun.*, 2017, **53**, 12564–12567.
18 Y. Niihori, S. Miyajima, A. Ikeda, T. Kosaka and Y. Negishi, *Small Sci.*, 2023, **3**, 2300024.
19 S. Miyajima, S. Hossain, A. Ikeda, T. Kosaka, T. Kawawaki, Y. Niihori, T. Iwasa, T. Taketsugu and Y. Negishi, *Commun. Chem.*, 2023, **6**, 57.
20 K. Nobusada and T. Iwasa, *J. Phys. Chem. C*, 2007, **111**, 14279–14282.
21 B. K. Teo, X. Shi and H. Zhang, *J. Chem. Soc., Chem. Commun.*, 1992, 1195–1196.
22 B. K. Teo, X. Shi and H. Zhang, *J. Am. Chem. Soc.*, 1991, **113**, 4329–4331.
23 B. K. Teo, H. Zhang and X. Shi, *Inorg. Chem.*, 1990, **29**, 2083–2091.
24 B. K. Teo, X. Shi and H. Zhang, *J. Cluster Sci.*, 1993, **4**, 471–476.
25 Z. Qin, J. Zhang, C. Wan, S. Liu, H. Abroshan, R. Jin and G. Li, *Nat. Commun.*, 2020, **11**, 6019.
26 B. K. Teo and H. Zhang, *Angew. Chem., Int. Ed. Engl.*, 1992, **31**, 445–447.
27 C. Zhou, P. Pan, X. Wei, Z. Lin, C. Chen, X. Kang and M. Zhu, *Nanoscale Horiz.*, 2022, **7**, 1397–1403.

28 B. K. Teo, H. Dang, C. F. Campana and H. Zhang, *Polyhedron*, 1998, **17**, 617–621.
29 X. Lin, J. Tang, J. Zhang, Y. Yang, X. Ren, C. Liu and J. Huang, *J. Chem. Phys.*, 2021, **155**, 074301.
30 H. Qian, W. T. Eckenhoff, Y. Zhu, T. Pintauer and R. Jin, *J. Am. Chem. Soc.*, 2010, **132**, 8280–8281.
31 L. Xu, Q. Li, T. Li, J. Chai, S. Yang and M. Zhu, *Inorg. Chem. Front.*, 2021, **8**, 4820–4827.
32 Y. Negishi, K. Igarashi, K. Munakata, W. Ohgake and K. Nobusada, *Chem. Commun.*, 2012, **48**, 660–662.
33 E. Ito, S. Ito, S. Takano, T. Nakamura and T. Tsukuda, *JACS Au*, 2022, **2**, 2627–2634.
34 I. Dolamic, S. Knoppe, A. Dass and T. Bürgi, *Nat. Commun.*, 2012, **3**, 798.
35 R. Saito, K. Isozaki, Y. Mizuhata and M. Nakamura, *J. Am. Chem. Soc.*, 2024, **146**, 20930–20936.
36 C. B. Murray, C. R. Kagan and M. G. Bawendi, *Science*, 1995, **270**, 1335–1338.
37 R. L. Whetten, J. T. Khoury, M. M. Alvarez, S. Murthy, I. Vezmar, Z. L. Wang, P. W. Stephens, C. L. Cleveland, W. D. Luedtke and U. Landman, *Adv. Mater.*, 1996, **8**, 428–433.
38 B. Yoon, W. D. Luedtke, R. N. Barnett, J. Gao, A. Desireddy, B. E. Conn, T. Bigioni and U. Landman, *Nat. Mater.*, 2014, **13**, 807–811.
39 H. Li, X. Kang and M. Zhu, *Acc. Chem. Res.*, 2024, **57**, 3194–3205.
40 C. Wang, X. Bu, N. Zheng and P. Feng, *J. Am. Chem. Soc.*, 2002, **124**, 10268–10269.
41 D. Wang, P. Wang, Z. Liang, Z. Li, N. Liu and Q. Ma, *Chem. Eng. J.*, 2023, **478**, 147512.
42 N. K. Chaki and K. P. Vijayamohanan, *J. Phys. Chem. B*, 2005, **109**, 2552–2558.
43 Y. Saito, Y. Shichibu and K. Konishi, *Nanoscale*, 2021, **13**, 9971–9977.
44 T. Sekine, J. Sakai, Y. Horita, H. Mabuchi, T. Irie, S. Hossain, T. Kawawaki, S. Das, S. Takahashi, S. Das and Y. Negishi, *Chem. – Eur. J.*, 2023, **29**, e202300706.
45 S. Das, T. Sekine, H. Mabuchi, S. Hossain, S. Das, S. Aoki, S. Takahashi and Y. Negishi, *Chem. Commun.*, 2023, **59**, 4000–4003.
46 J. Sakai, S. Biswas, T. Irie, H. Mabuchi, T. Sekine, Y. Niihori, S. Das and Y. Negishi, *Nanoscale*, 2023, **15**, 12227–12234.
47 R. Nakatani, S. Biswas, T. Irie, J. Sakai, D. Hirayama, T. Kawawaki, Y. Niihori, S. Das and Y. Negishi, *Nanoscale*, 2023, **15**, 16299–16306.
48 Z. Wang, Y.-J. Zhu, Y.-Z. Li, G.-L. Zhuang, K.-P. Song, Z.-Y. Gao, J.-M. Dou, M. Kurmoo, C.-H. Tung and D. Sun, *Nat. Commun.*, 2022, **13**, 1802.
49 Y.-P. Xie, J.-L. Jin, G.-X. Duan, X. Lu and T. C. W. Mak, *Coord. Chem. Rev.*, 2017, **331**, 54–72.
50 L.-M. Zhang and T. C. W. Mak, *J. Am. Chem. Soc.*, 2016, **138**, 2909–2912.
51 T. Higaki, Y. Li, S. Zhao, Q. Li, S. Li, X.-S. Du, S. Yang, J. Chai and R. Jin, *Angew. Chem., Int. Ed.*, 2019, **58**, 8291–8302.
52 T. Chen, S. Yang, Q. Li, Y. Song, G. Li, J. Chai and M. Zhu, *Nanoscale Horiz.*, 2021, **6**, 913–917.
53 T. Higaki, C. Liu, C. Zeng, R. Jin, Y. Chen, N. L. Rosi and R. Jin, *Angew. Chem., Int. Ed.*, 2016, **55**, 6694–6697.
54 Z.-R. Wen, Z.-J. Guan, Y. Zhang, Y.-M. Lin and Q.-M. Wang, *Chem. Commun.*, 2019, **55**, 12992–12995.
55 M. Sugiuchi, Y. Shichibu, T. Nakanishi, Y. Hasegawa and K. Konishi, *Chem. Commun.*, 2015, **51**, 13519–13522.
56 Y. Fukumoto, T. Omoda, H. Hirai, S. Takano, K. Harano and T. Tsukuda, *Angew. Chem., Int. Ed.*, 2024, **63**, e202402025.
57 C. A. Hosier, I. D. Anderson and C. J. Ackerson, *Nanoscale*, 2020, **12**, 6239–6242.
58 X.-K. Wan, J.-Q. Wang, Z.-A. Nan and Q.-M. Wang, *Sci. Adv.*, 2017, **3**, e1701823.
59 Q. Tang and D.-E. Jiang, *J. Phys. Chem. C*, 2015, **119**, 10804–10810.
60 Q. Tang and D.-E. Jiang, *Chem. Mater.*, 2017, **29**, 6908–6915.
61 F. Bejarano, I. J. Olavarria-Contreras, A. Droghetti, I. Rungger, A. Rudnev, D. Gutiérrez, M. Mas-Torrent, J. Veciana, H. S. J. van der Zant, C. Rovira, E. Burzurí and N. Crivillers, *J. Am. Chem. Soc.*, 2018, **140**, 1691–1696.
62 X.-K. Wan, Z.-J. Guan and Q.-M. Wang, *Angew. Chem., Int. Ed.*, 2017, **56**, 11494–11497.
63 T. Zaba, A. Noworolska, C. M. Bowers, B. Breiten, G. M. Whitesides and P. Cyganik, *J. Am. Chem. Soc.*, 2014, **136**, 11918–11921.
64 K. P. Hall and D. M. P. Mingos, *Prog. Inorg. Chem.*, 1984, **32**, 237–325.
65 P. Maity, T. Wakabayashi, N. Ichikuni, H. Tsunoyama, S. Xie, M. Yamauchi and T. Tsukuda, *Chem. Commun.*, 2012, **48**, 6085–6087.
66 P. Maity, S. Takano, S. Yamazoe, T. Wakabayashi and T. Tsukuda, *J. Am. Chem. Soc.*, 2013, **135**, 9450–9457.
67 N. Kobayashi, Y. Kamei, Y. Shichibu and K. Konishi, *J. Am. Chem. Soc.*, 2013, **135**, 16078–16081.
68 N. Kito, S. Takano, S. Masuda, K. Harano and T. Tsukuda, *Bull. Chem. Soc. Jpn.*, 2023, **96**, 1045–1051.
69 A. Leyva-Pérez, A. Doménech-Carbó and A. Corma, *Nat. Commun.*, 2015, **6**, 6703.
70 L. Wang, R. Liu, J. Gu, B. Song, H. Wang, X. Jiang, K. Zhang, X. Han, X.-Q. Hao, S. Bai, M. Wang, X. Li, B. Xu and X. Li, *J. Am. Chem. Soc.*, 2018, **140**, 14087–14096.
71 S.-Y. Zhang, H.-Y. Sun, R.-G. Wang, Y.-S. Meng, T. Liu and Y.-Y. Zhu, *Dalton Trans.*, 2022, **51**, 9888–9893.
72 E. C. Constable, J. Lewis, M. C. Liptrot and P. R. Raithby, *Inorg. Chim. Acta*, 1990, **178**, 47–54.
73 J. Kožíšek, J. Svoboda, J. Zedník, B. Vlčková and I. Šloufová, *J. Phys. Chem. B*, 2021, **125**, 12847–12858.
74 R. H. Holyer, C. D. Hubbard, S. F. A. Kettle and R. G. Wilkins, *Inorg. Chem.*, 1965, **4**, 929–935.
75 B. Valeur and M. N. Berberan-Santos, in *Molecular Fluorescence*, Wiley-VCH, 2012, ch. 8, pp. 213–261.
76 Y. Niihori, W. Kurashige, M. Matsuzaki and Y. Negishi, *Nanoscale*, 2013, **5**, 508–512.

 

77 Y. Niihori, Y. Kikuchi, A. Kato, M. Matsuzaki and Y. Negishi, *ACS Nano*, 2015, **9**, 9347–9356.
78 Y. Niihori, M. Eguro, A. Kato, S. Sharma, B. Kumar, W. Kurashige, K. Nobusada and Y. Negishi, *J. Phys. Chem. C*, 2016, **120**, 14301–14309.
79 Y. Wang and T. Bürgi, *Nanoscale Adv.*, 2021, **3**, 2710–2727.
80 W. Suzuki, R. Takahata, Y. Chiga, S. Kikkawa, S. Yamazoe, Y. Mizuhata, N. Tokitoh and T. Teranishi, *J. Am. Chem. Soc.*, 2022, **144**, 12310–12320.